Materials and Structures (2017)50:173
DOI 10.1617/s11527-017-1042-6

ORIGINAL ARTICLE

Low-temperature curing strength enhancement in cement-based materials containing limestone powder

Dale P. Bentz · Paul E. Stutzman · Franco Zunino

Received: 1 November 2016 / Accepted: 24 April 2017

Abstract With the ongoing sustainability movement, the incorporation of limestone powder in cementitious binders for concrete in the U.S. has become a subject of renewed interest. In addition to accelerating the early age hydration reactions of cementitious systems by providing additional surfaces for nucleation and growth of products, limestone powder is also intriguing based on its influence on low-temperature curing. For example, previous results have indicated that the utilization of limestone powder to replace one quarter of the fly ash in a high volume fly ash mixture (40–60% cement replacement) produces a reduction in the apparent activation energy for setting for temperatures below 25 °C. In the present study, the relationship between heat release and compressive strength of mortars at batching/curing temperatures of 10 and 23 °C is investigated. For Portland-limestone cements (PLC) with limestone additions on the order of 10%, a higher strength per unit heat release is obtained after only 7 d of curing in lime water. Surprisingly, in some cases, the absolute strength of these mortar cubes measured at 7 d is higher when cured at 10 °C than at 23 °C. Solubilities vs. temperature, reaction stoichiometries and enthalpies, and projected phase distributions based on thermodynamic modeling for the cementitious phases are examined to provide some theoretical insight into this strength enhancement. For a subset of the investigated cements, thermogravimetric analysis, quantitative X-ray diffraction, and scanning electron microscopy are conducted on 7-d paste specimens produced at the two temperatures to examine differences in their reaction rates and the phases produced. The strength enhancement observed in the PLC cements is related to the cement hydration products formed in the presence of carbonates as a function of temperature.

Keywords Compressive strength · Heat release · Limestone powder · Low-temperature curing · Thermodynamics · X-ray diffraction

D. P. Bentz (✉) · P. E. Stutzman
Engineering Laboratory, National Institute of Standards and Technology, 100 Bureau Drive, Stop 8615, Gaithersburg, MD 20899-8615, USA
e-mail: dale.bentz@nist.gov

P. E. Stutzman
e-mail: paul.stutzman@nist.gov

F. Zunino
Faculty of Engineering, Universidad del Desarrollo, Avenida La Plaza 680, Las Condes, Santiago, Chile
e-mail: f.zunino@udd.cl; franco.zunino@epfl.ch

Present Address:
F. Zunino
Laboratory of Construction Materials, EPFL-STI-IMX-LMC, Station 12, 1015 Lausanne, Switzerland

Published online: 28 April 2017

1 Introduction

The sustainability-driven quest to replace a significant portion of portland cement in concrete with other materials has led to renewed interest in limestone powders as an effective accelerator of early-age hydration and beneficial modifier of rheology [1–9]. The addition of (calcium) carbonate to the cementitious system changes the phase equilibria and its temperature dependence. Like calcium hydroxide, all three polymorphs of $CaCO_3$ (calcite, aragonite, and vaterite) exhibit a solubility that increases with decreasing temperature [10], unlike most commonly available minerals. One of the important outcomes of these influences is that for some cement-based materials containing limestone powder, after 7 d of curing, the strength achieved at 10 °C exceeds that obtained at 23 °C (see Fig. 1 for two such examples from a recent study [8]). While it is well known that low-temperature curing can produce higher ultimate strengths [12], perhaps due to the formation of a lower density calcium silicate hydrate gel (C–S–H) [13], observing a crossover after only 7 d is a bit extreme. The purpose of the present study is to further investigate this surprising behavior.

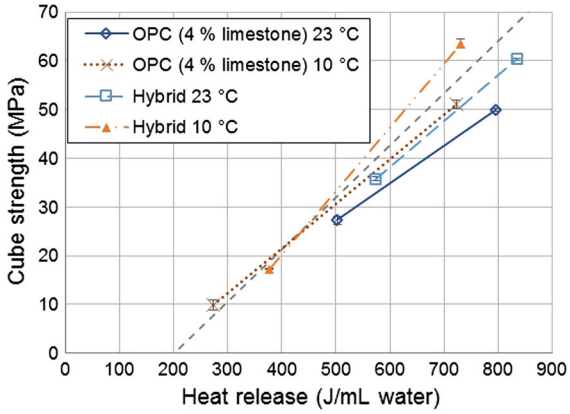

Fig. 1 Mortar cube compressive strength versus heat release per unit volume of water for an ASTM C150 Type I/II ordinary portland cement with a 4% limestone addition and for a hybrid mortar containing 20% limestone and 1% $CaCl_2$ (both replacing sand) by mass of cement, cured at 10 or 23 °C (data from reference [8]). *Error bars* indicate ±one standard deviation in measured compressive strength for 3 cube specimens. *Dashed grey line* extending from (200, 0) to (850, 70) indicates strength-heat release relationship found for mortars in a previous study [11]. At 7 d, absolute strength value is slightly higher for both mortars cured at 10 °C than for the corresponding ones cured at 23 °C

2 Thermochemical properties and reactions

A good starting point for an investigation into strength differences is to consider the inherent dependence of strength on porosity [14, 15] and investigate possible porosity differences with temperature, due to the reactions occurring and the phases being consumed and produced. Because mortars containing limestone powder exhibit this low temperature strength enhancement while those without it do not, the focus here will be on the interaction of carbonates with calcium aluminate phases and not on the hydration of calcium silicates to produce C–S–H and calcium hydroxide. While the calcite form of $CaCO_3$ significantly accelerates early hydration of these silicate phases [4, 6–9, 15], for a system containing the same proportion of $CaCO_3$, this acceleration would not offer a viable explanation of low temperature strength enhancement (as in fact the opposite behavior might be expected). Additionally, the reactivity of the ferrite phase (C_4AF) will not be considered in detail at this first stage of analysis, although the incorporation of iron into carbonate containing AFm phases has been examined previously [16].

The relevant thermochemical properties of a variety of cementitious phases of interest to the present study are summarized in Table 1 [17–21]. In conventional ordinary portland cements (OPCs) without limestone additions, the aluminates will generally interact with sulfate sources (gypsum, hemihydrate, and/or anhydrite) to form ettringite and monosulfoaluminate phases, and can also form calcium aluminate hydrates such as hydrogarnet when sufficient sulfate is not readily available. Generally, ettringite forms first and then converts to monosulfate as sulfate ions in the pore solution become depleted [20]. In reality, even for systems without a limestone powder addition, some carbonate is usually provided by the curing environment, so that trace amounts of hemicarbonate (HC) and monocarbonate (MC) phases are often detected, as well as being more prevalent in the systems with intentional limestone powder additions. These carbonates can also indirectly stabilize the presence of ettringite, eliminating its conversion to monosulfate [1, 15, 22]. For completeness, several chloride-containing phases are also included in Table 1, although they are not the focus of the present study.

Due to the inherent relationship between porosity and strength [14, 15] and the general proportionality

Table 1 Thermochemical and reaction (one mole of C_3A basis) properties of cementitious phases [17–21]

Phase	Chemical formula[a]	Molar volume (cm^3/mole)	Density (kg/m^3)	Heat of formation (kJ/mole)	Formation reaction equation	Solids volume produced (cm^3/mole)|Expansion factor (solids basis)	Heat released (kJ/mole)	Volume/heat (cm^3/kJ)
Monosulfoaluminate	$C_4A\overline{S}H_{12}$	312.82	1990	−8778	$C_3A + C\overline{S}H_2 + 10H \rightarrow C_4A\overline{S}H_{12}$	149.7|1.92	309.4	0.484
Monocarbonate (MC)	$C_4A\overline{C}H_{11}$	261.91	2170	−8184	$C_3A + C\overline{C} + 11H \rightarrow C_4A\overline{C}H_{11}$	136.0|2.08	245.3	0.555
Hemicarbonate (HC)	$C_4A\overline{C}_{0.5}H_{12}$	350.8	1980	−8270	$C_3A + 0.5C\overline{C} + 0.5 CH + 11.5H \rightarrow C_4A\overline{C}_{0.5}H_{12}$	226.9|2.83	298.8	0.759
Ettringite	$C_6A\overline{S}_3H_{32}$	735.01	1707.6	−17,539	$C_3A + 3C\overline{S}H_2 + 26H \rightarrow C_6A\overline{S}_3H_{32}$	423.4|2.36	452.1	0.937
Friedel's salt	$C_3A(CaCl_2)H_{10}$	296.66	1892	−7670.04	$C_3A + CaCl_2{\cdot}2H + 8H \rightarrow C_3ACaCl_2H_{10}$	128.3|1.76	391.6	0.328
Calcium chloride dihydrate	$(CaCl_2){\cdot}2H$	79.47	1850	−1404.07				
Calcite (limestone)	$C\overline{C}$	36.93	2710	−1206.92				
Calcium hydroxide	CH	33.1	2240	−986.1				
Gypsum	$C\overline{S}H_2$	74.21	2320	−2022.6				
Tricalcium aluminate	C_3A	88.94	3038	−3587.8				
Hydrogarnet	C_3AH_6	150.12	2520	−5560				

[a] Conventional cement chemistry notation is used here and elsewhere, except for calcium chloride ($CaCl_2$): C = CaO, $\overline{S}$ = SO_3, A = Al_2O_3, F = Fe_2O_3, H = H_2O, and $\overline{C}$ = CO_2

between heat release (as a measure of degree of reaction) and porosity reduction, when mortar strength is plotted vs. heat release normalized by the starting volume of water, a linear relationship is consistently obtained, as already illustrated in Fig. 1 [11]. Based on the thermochemical properties and assumed reactions provided in Table 1, one can calculate the ratio of the additional solids volume generated to the heat released, each on a mole of tricalcium aluminate (C_3A) basis, for example. The results in Table 1 are quite informative in that the formation of MC results in about a 15% increase in the solids volume generated per unit heat release relative to that produced by conventional monosulfate formation, while the value for HC formation exhibits an even greater 57% increase. The increase for ettringite formation is highest at 94%. Conversely, the formation of Friedel's salt yields about a 32% decrease. Relative to monosulfate, the absolute expansions factors (solids basis) for the other phases are 8.5% higher, 47.6% higher, 23.0% higher, and 8.1% lower for MC, HC, ettringite, and Friedel's salt, respectively. Based on these calculations, enhanced formation of carbonate phases (particularly HC) and their indirect stabilization of ettringite could indeed lead to a lower porosity and higher strength cement paste [22], on both absolute and per unit heat release bases. In addition to the porosity reduction, carboaluminate phases are generally stiffer than the corresponding sulfoaluminates [23], which could also contribute to the observed strength enhancement.

An additional consideration is the solubility of the calcite polymorph of limestone as a function of temperature that is given by Plummer and Busenberg [10] as:

$$\log(K_{sp}) = -171.9065 - 0.077993T + 2839.319/T + 71.595\log(T) \quad (1)$$

where T is in K. This equation implies that the solubility of calcite at 10 °C would be 14% higher than that at 23 °C and 48% higher than that at 40 °C. This enhanced solubility at lower temperatures could also potentially contribute to increased reactivity and the observed strength enhancement.

3 Materials and experimental procedures

Four cements were obtained to investigate their sensitivity to (low) curing temperatures in the present study. Two contained substantial percentages of added limestone (LS), a white (only 0.36% Fe_2O_3) portland limestone cement (PLC) with about 12% LS and a second PLC (grey) with a manufacturer-reported LS addition rate of 10.36%. No information is available on the purity of the added limestone for either of these two cements, but generally for limestone powders added to cement, their $CaCO_3$ content is greater than 95%. It actually proved more difficult to find OPCs without limestone additions, as ASTM C150 [24] currently permits up to 5% interground limestone in OPC and most manufacturers take advantage of this cost-saving opportunity (limestone powder costing considerably less than portland cement), the OPC in Fig. 1 being one example of this trend. Eventually, two OPCs without LS additions were obtained, one from Chile (limestone percentage of about 1% as estimated by thermogravimetric analysis) and the other from a US manufacturer (limestone percentage of 0.1% based on cement carbon measurements [25]). Particle size distribution characteristics, helium pycnometry densities, and BET surface areas of the four cements, as measured at NIST, are provided in Table 2, along with X-ray fluorescence (XRF)-based oxide contents and quantitative XRD-estimated (Rietveld) phase compositions. The physical characteristics of the four cements are fairly similar, with the Chilean OPC being somewhat coarser; thus, the major difference is in their limestone ($C\overline{C}$) contents.

Mortar cubes based on each cement were prepared as described previously [8]. Batch proportions typically consisted of 781 g of cement, 441 g of fine silica sand, 335.5 g each of C778 graded and 20–30 sands, and 653 g of coarse silica sand, along with 312.4 g of water, for a water-to-cement ratio (w/c) by mass of 0.4. Mixing was performed following ASTM C305 [24], in a temperature-controlled environmental chamber set at either 10 or 23 °C, the same chamber also being used for the subsequent curing of the cubes in sealed containers of lime water. Starting materials were preconditioned at reduced temperatures to achieve temperatures after mixing that were consistently near the target curing temperature [8]. Three sets of mortar cubes (three cubes per set) were prepared for each mixture/temperature, demolded after 1 d, and then broken after 1, 7, or 28 d. Isothermal calorimetry, at either 10 or 23 °C was conducted on a small sample of prepared mortar (about 7.6 g) placed in a sealed

Table 2 Characteristics of the four cements (– indicates value was not measured/reported)

Cement	White PLC	PLC (10% LS)	Chilean OPC	US OPC
SiO_2 (mass%)	20.59	19.31	20.51	20.3 [25]
Al_2O_3 (mass%)	3.61	3.85	4.71	5.0
Fe_2O_3 (mass%)	0.36	3.48	3.12	–
CaO (mass%)	64.91	61.97	63.76	64.2
MgO (mass%)	1.65	2.51	1.23	–
SO_3 (mass%)	2.62	2.68	2.89	3.1
K_2O (mass%)	–	0.47	0.46	–
Na_2O (mass%)	–	0.24	0.53	–
TiO_2 (mass%)	–	0.16	0.23	–
D_{10}, D_{50}, D_{90} (μm)[a]	1.0, 8.3, 28.1	1.2, 8.4, 25.8	2.1, 15.5, 47.9	1.8, 11.8, 36.6
Density (kg/m^3)	3074 ± 1[C]	3112 ± 2	3135 ± 1	3140 ± 2
BET surface (m^2/g)[c]	2.02	1.59	1.05	1.07
C_3S (mass%)	–	64.4 ± 0.5[b]	69.2 ± 0.4	–
C_2S (mass%)	–	10.1 ± 0.4	11.7 ± 0.3	–
C_3A (mass%)	–	2.5 ± 0.2	7.4 ± 0.3	–
C_4AF (mass%)	–	11.6 ± 0.3	9.6 ± 0.4	–
$C\overline{S}$ (mass%)	–	3.0 ± 0.1	2.2 ± 0.1	–
$C\overline{C}$ (mass%)	–	8.6 ± 0.2	–	–

[a] D_{10}, D_{50}, and D_{90} correspond to the particle sizes for which the indicated % of particles (subscript) would be finer than. For three replicates for PLC (10% LS), coefficients of variation for D_{10}, D_{50}, and D_{90} were determined to be 0.3, 0.9, and 0.5%, respectively

[b] Uncertainty represents one standard deviation for three replicate specimens

[c] Typical coefficient of variation of 2% for three replicate specimens [26]

glass vial and monitored for a period of 7 d. For calorimetry measurements, the average absolute difference between replicate specimens was previously measured to be 2.4×10^{-5} W/g (cement), for measurements conducted between 1 h and 7 d after mixing [27].

For the Chilean OPC and the PLC (10% LS) cements, further studies were conducted on $w/c = 0.4$ paste specimens prepared in a temperature-controlled (water–cooled) blender following ASTM C1738 [24]. Specimens were placed in sealed cylindrical plastic vials with a small volume of water on top to maintain saturated curing conditions and placed in a temperature-controlled environmental chamber. After 7 d of curing, samples from the specimens were obtained for thermogravimetric analysis (TGA), quantitative X-ray diffraction (XRD), and scanning electron microscopy (SEM). For a TGA scan, the system was equilibrated at 30 °C and then the temperature was raised to 1000 °C at a rate of 10 °C/min, while flushing with ultra-high purity nitrogen at a flow rate of 50 mL/min. Sample size for the TGA varied between about 50 mg and 100 mg. A similar TGA analysis was also conducted on the initial dry powders for these two cements.

In addition to the TGA analysis, the 7 d specimens were also subjected to XRD and SEM analyses to assess their hydration product types and textures. Two disks approximately 25 mm in diameter and 1 mm thick were wafered from the cylinders with a diamond saw, using ethanol as the cutting lubricant. The specimen intended for SEM analysis was dried at 60 °C and embedded with an ultra-low viscosity resin [28] for subsequent imaging in the scanning electron microscope. The specimens were subsequently ground to expose the paste surface and polished using a set of successively finer diamond paste compounds of 6, 3, 1, and 0.25 μm, finally being coated with a film of deposited carbon to provide a conductive surface for SEM imaging.

The second wafer intended for X-ray powder diffraction analysis was lapped using 600–grit silicon carbide paper followed by 1200-grit paper, to provide a smooth surface necessary for XRD analysis. The paste specimen was analyzed intact rather than as a powder to avoid possible alteration due to crushing and grinding. The paste specimens for XRD were scanned from 4° 2θ to 65° 2θ with a step of 0.016° 2θ and total collection time of 30 min. The diffraction pattern phase identifications were facilitated by using

the ICDD diffraction database,[1,2] and the Highway Research Board data on X-ray identification of hydration products [29].

4 Thermodynamic modeling of phase distributions versus temperature and cement composition

To further explore the influence of temperature on phase assemblage and volume fractions, thermodynamic modeling was conducted using the Gibbs energy minimization method (GEMS). For this purpose, GEMS version 3 Software[3] was employed [30, 31], coupled with the CEMDATA14[4] thermodynamic database. Thermodynamic modeling using this method has proven to be a useful tool to understand the phase assemblage of cementitious systems containing $C\overline{C}$ additions and hydrated at different temperatures [1, 32, 33].

The Chilean OPC and the PLC (10% LS) were modeled based on their phase composition (Table 2), as determined by XRD and Rietveld refinement. The four main clinker phases (C_3S, C_2S, C_3A and C_4AF) were considered, as well as gypsum and the $C\overline{C}$ addition. The amount of MgO as determined by XRF was also accounted for in both systems. A *w/c* of 0.4 was used to be consistent with the experimental systems, by modeling a mixture of 100 g of cement with 40 g of water. The model was run between 5 and 25 °C in 1 °C increments to assess the influence of temperature on phase assemblage and relative volumes. Since the internal porosity of C–S–H is neglected by the model, the molar amount produced at equilibrium was multiplied by a molar volume of 108 cm^3/mol [20] to obtain its volumetric fraction. The volumes of the other hydration products were taken directly from the modeling results, and all the molar volumes were checked to be within 1% of the values presented in Table 1.

In addition, the Chilean OPC phase composition was considered as a base system, and different amounts of $C\overline{C}$ replacements varying from 1 to 15% by mass were added, while keeping *w/c* (limestone powder considered as part of cement) constant at 0.4. The model was run in the same temperature range and increments, to better understand the influence of $C\overline{C}$ on the total volume of solids at thermodynamic equilibrium at different curing temperatures.

5 Results and discussion

5.1 Strength versus heat release

The measured compressive strengths for the four cements at two curing temperatures and three ages are summarized in Table 3. As would be expected, at 1 d, the strengths produced via 23 °C curing far exceed those obtained at 10 °C, by about a factor of 2.5. These differences in strength are narrowed considerably by 7 d, and for the PLC (10% LS) system, the 10 °C curing provides slightly superior strengths at both 7 d and 28 d.

A more informative view of the data is obtained by plotting measured compressive strength vs. heat release normalized per unit volume of water, as shown in Fig. 2. As first presented in Table 1, the formation of different phases from the reaction of C_3A leads to different values for the ratio of formed solids volume to heat release (roughly indicated by the slope in Fig. 2). When the compressive strengths measured at the two curing temperatures are plotted against heat release, two types of general behavior are clearly observed. For the cements without LS additions, all of the results fall in close proximity to a single line (constant slope), implying a similar phase distribution being produced at each curing temperature, albeit at quite different rates. Conversely, for the two cements with significant LS additions, the 10 and 23 °C lines diverge, with the cube strength per unit heat release being greater in the former case, particularly for the 7 d data in each case. This implies a more variable phase distribution with temperature and the values in Table 1 would suggest this difference to likely be due to the presence of additional HC at the lower curing

[1] Powder Diffraction Database, International Center for Diffraction Data, http://www.icdd.com.

[2] Certain commercial equipment and software are identified to describe the subject adequately. Such identification does not imply recommendation or endorsement by NIST, nor does it imply that the equipment identified is necessarily the best available for the purpose.

[3] Available at http://gems.web.psi.ch.

[4] Available for free from EMPA at https://www.empa.ch/web/s308/cemdata.

Table 3 Compressive strength results for mortar cubes

Cement, Temperature	1 d strength (MPa)	7 d strength (MPa)	28 d strength (MPa)
White PLC at 10 °C	13.0 (4.7%)[a]	56.9 (2.8%)	63.5 (1.1%)
White PLC at 23 °C	35.3 (3.2%)	59.6 (4.5%)	71 (1.0%)
PLC (10% LS) at 10 °C	15.1 (3.6%)	52.8 (3.1%)	61.0
PLC (10% LS) at 23 °C	34.5 (6.9%)	52.1 (2.9%)	60.2 (6.6%)
Chilean OPC at 10 °C	10.2 (0.9%)	47.3 (1.6%)	55.5 (2.1%)
Chilean OPC at 23 °C	28.8 (2.4%)	50.2 (2.4%)	59.2 (1.4%)
(with repeat)	28.8 (1.4%)	49.7 (4.9%)	60.3 (2.5%)
US OPC at 10 °C	12.2 (1.1%)	44.8 (4.6%)	60.8 (1.2%)
US OPC at 23 °C	29.5 (1.1%)	53.0 (3.2%)	65.3 (2.8%)

[a] Numbers in parentheses indicates coefficient of variation for testing three specimens

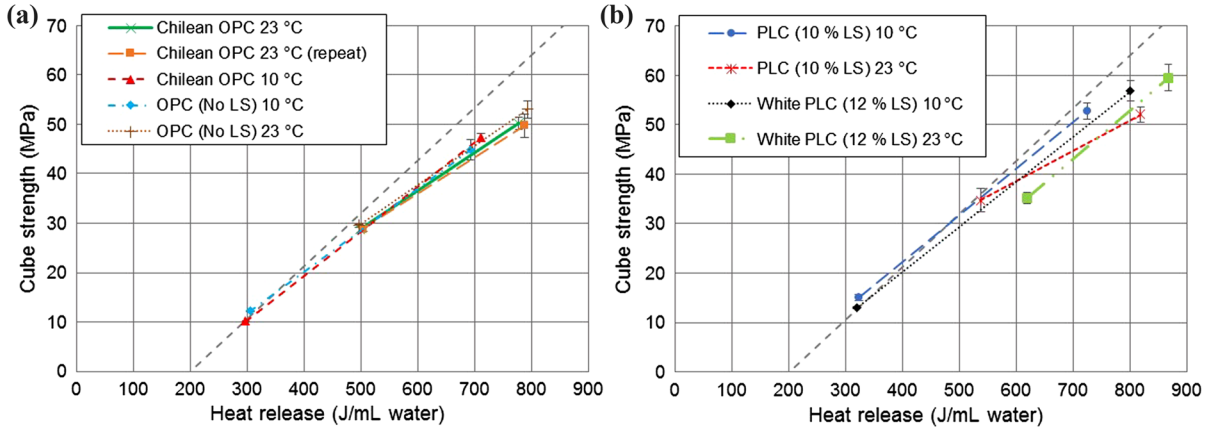

Fig. 2 Cube compressive strength versus heat release per unit volume of water for specimens cured at two temperatures and tested after 1 and 7 d for: **a** Chilean OPC with no LS and (US) OPC with no LS and **b** PLC (10% LS) and white PLC (12% LS). For each plot, *dashed grey line* indicates strength-heat release relationship found for mortars in a previous study [11]

temperature, along with the possible enhanced stabilization of ettringite. This hypothesis was further explored via TGA, XRD, and SEM analysis, along with the thermodynamic modeling, as discussed in the sections to follow.

5.2 Thermogravimetric analysis

The results of the TGA analysis performed on the 7 d specimens of Chilean OPC and PLC (10% LS) are provided in Fig. 3. For each cement, the TGA scans at the two temperatures are fairly similar. The reactivity of the $C\overline{C}$ in the PLC is observed based on the change in the peaks observed in the temperature range of 550–775 °C for the powder vs. the two hydrated specimens. The $C\overline{C}$ estimate of 8.8 ± 0.3% (three replicates, non-ignited basis assuming 100% pure $C\overline{C}$) for the PLC powder is in reasonable agreement with the 10.36% value (non-ignited basis, purity unknown) provided by its manufacturer and the 8.6% provided by XRD analysis (Table 2). A quantitative analysis of the percentage of the original $C\overline{C}$ reacted in the hydrated systems (based on mass loss from 600 to 775 °C, ignited basis) yields estimates of 7.9 and 7.6% for the 10 and 23 °C cured systems, respectively. While this would be consistent with the increased solubility of calcite at lower temperatures, this difference between the two values is not statistically significant, based on replicate measurements on the cement powder quoted above, along with those from a previous study [5].

For the two cements, the TGA scans after hydration at 10 and 23 °C are quite similar, with some minor differences in those temperature ranges where calcium hydroxide (400–550 °C) or C-S-H/sulfoaluminate hydration products (50 –250 °C) are indicated. The additional mass loss in the latter range for

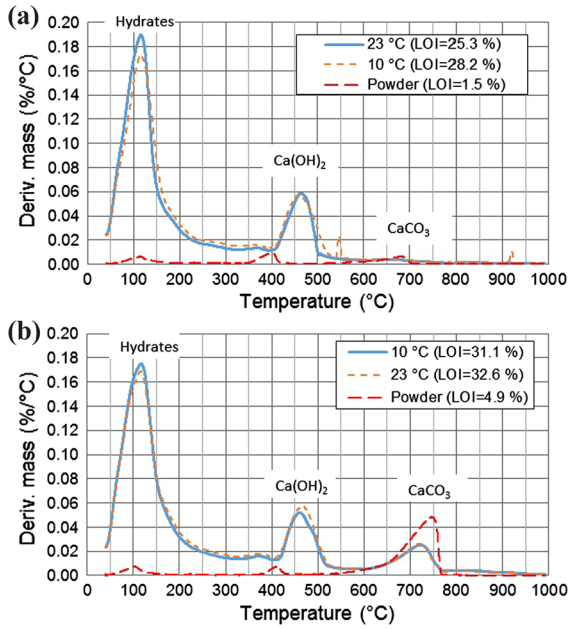

Fig. 3 TGA derivative mass versus temperature for **a** Chilean OPC with no LS and **b** PLC (10% LS), both cured for 7 d in lime water. Loss on ignition (LOI) indicates mass loss between 100 and 1000 °C on a per g ignited basis

the PLC cured at 10 °C would be consistent with the higher water content (per mole of C_3A) of HC and ettringite relative to monosulfate (Table 1), but the observed difference could also be caused by differences in the density and water content of the C–S–H hydration product [13, 34]. The latter may be more likely considering that a similar or perhaps even slightly more pronounced difference is observed in the Chilean OPC with no LS addition. The measured LOI for the different mixtures is included in the legends in Fig. 3 and while the 10 and 23 °C values are more similar for the PLC than for the Chilean OPC, in both cases a greater total TGA mass loss was observed for the system hydrated at 23 °C. Since the TGA results were somewhat inconclusive in this regard, further investigations using XRD and SEM were performed.

5.3 Quantitative X-ray diffraction

The measured XRD patterns for the two cements hydrated at both curing temperatures are provided in Fig. 4. The PLC (10% LS) pastes at both 10 °C and 23 °C curing exhibit 0.812 nm (001, at $2\theta \approx 11°$) and 0.406 nm (002, at $2\theta \approx 22°$) diffraction peaks (d-spacing) that correspond to $C_4A\,\overline{C}_{0.5}H_{12}$ (HC) (Fig. 4). The 23 C paste additionally has a 0.756 nm (11.7°) peak corresponding to $C_4A\,\overline{C}H_{11}$ (MC). According to the values provided in Table 1, for an equal number of moles of C_3A reacted, the volumetric expansion generated would be significantly greater in the case of HC production in comparison to MC. An even larger increase in expansion would be present for the case of equal moles of $C\overline{C}$ reacted (assuming sufficient C_3A is available in each case and supported by the TGA results in Fig. 3b), since one mole of $C\overline{C}$ forms two moles of HC, but only one mole of MC. So, the XRD results for the PLC (10% LS) cement in Fig. 4 are indeed consistent with the previous hypothesis concerning enhanced HC formation (and less MC) at the lower curing temperature. In addition, and as will be discussed in the thermodynamic modeling results to follow, the uptake of CO_3^{2-} by ettringite increases at low temperature, further increasing the volumetric expansion of the solids formed.

Portlandite (CH) contents for the PLC pastes appear similar, with the 10 °C paste possibly having stronger (remaining) alite (C_3S) peak intensities. Alite content is lowest for the 23 °C PLC cement, and for both curing temperatures is lower than those for the Chilean OPC cement, not unexpectedly. Peak intensities for portlandite and ettringite between the two curing temperatures appear similar, with a minor indication of increased ettringite peak heights for the PLC cured at 10 °C, particularly for the peak at about 9.2° 2θ in Fig. 4. As indicated previously, enhanced ettringite formation could be one contributor to the enhanced strength (reduced porosity) observed at lower curing temperatures in this study.

In contrast, the Chilean OPC cement pastes at both curing temperatures exhibit a broad, lower-intensity HC peak centered around 0.812 nm reflecting more disorder and, for the 23 °C paste, evidence of a 0.756 nm peak corresponding to MC. The minor $C\overline{C}$ content of the Chilean OPC and CO_2 from the environment are hypothesized as equally likely sources for the formation of these minor carbonates. While ettringite and AFm phase contents appear similar between the two curing temperatures, the 10 °C specimen appears to have slightly more portlandite.

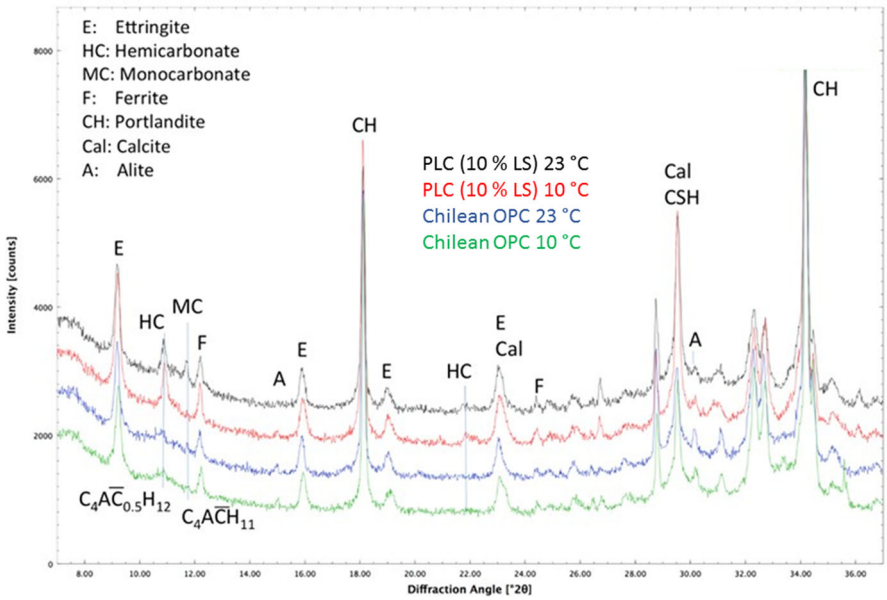

Fig. 4 Low angle region of the 7-d X-ray powder diffraction patterns illustrates differences in HC and MC phases with sharper, better-ordered HC and MC in pastes from limestone-containing cement at both 10 and 23 °C. Patterns from bottom to top are Chilean OPC at 10 °C, Chilean OPC at 23 °C, PLC (10% LS) at 10 °C, and PLC (10% LS) at 23 °C

5.4 Scanning electron microscopy

Representative SEM images for the paste microstructures produced at the two curing temperatures are provided in Figs. 5, 6 for the Chilean OPC and the PLC (10% LS), respectively. For a given cement, the microstructures at the two curing temperatures appear quite similar, in agreement with their similar heat release values (x-axis of Fig. 2), TGA curves (Fig. 3), and XRD patterns (Fig. 4, particularly for the Chilean OPC). Still, two features do stand out in comparing these sets of images. First, the cement pastes that contain LS appear to have a finer-sized, more uniformly-distributed portlandite in both the 10 and 23 °C pastes, perhaps due to additional calcium ions emanating from the initial dissolution of a very small quantity of the $C\overline{C}$ at early ages. Second, the 10 °C PLC (10% LS) paste (most prominently the C–S–H) appears denser than its 23 °C counterpart and the Chilean OPC pastes at both curing temperatures. However, X-ray microanalysis of the outer product C–S–H between specimens did not reveal any consistent or distinct compositional differences.

5.5 Interpretation via thermodynamic modeling

Figures 7 and 8 show the predicted solid phase volumes at equilibrium for the Chilean OPC and PLC (10% LS) cements respectively, at curing temperatures between 5 and 25 °C. Regarding the Chilean OPC system, in addition to the usual hydration products formed from the reactions of C_3S, C_2S, and C_3A with water (i.e., C–S–H, portlandite, and AFt), a solid solution hydrogarnet ($C_3(A,F)S_{0.84}H_{4.32}$) is observed, as well as hydrotalcite, due to the consideration of MgO in the composition of the cement. HC and MC are also observed at all temperatures due to the presence of 1% of $C\overline{C}$ in the system, consistent with the SO_3/Al_2O_3 (0.90) and CO_2/Al_2O_3 (0.43) molar ratios of this cement [1]. Previous studies have shown that $C_3FS_{0.84}H_{4.32}$ is the most stable iron-containing phase in hydrated portland cement [35]. It can be observed in Fig. 7 that the total volume of solid phases remains almost constant between low and higher temperatures. The amount of portlandite generated decreases with temperature, while that of C–S–H slightly increases as the temperature decreases. The total volume of solids difference between the 5 and 25 °C systems is only −0.086%.

In the PLC (10% LS) system, additional phases are formed due to the presence of $C\overline{C}$ (calcite). MC is observed, which is consistent with the expected phase assemblage for the SO_3/Al_2O_3 (0.53) and CO_2/Al_2O_3 (1.13) molar ratios of this particular cement [1, 32]. In addition, the AFt phase is composed of a solid solution of SO_3^{2-} (ettringite) and CO_3^{2-} (tricarboaluminate)

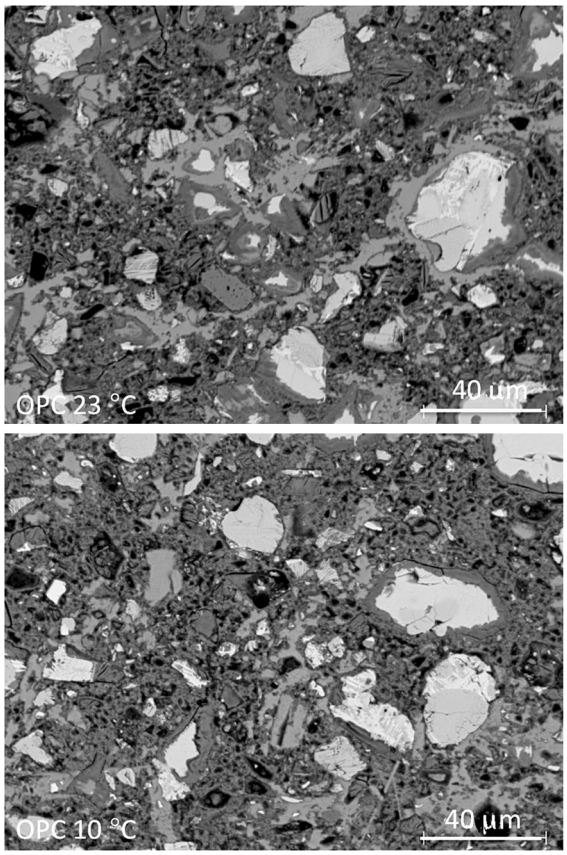

Fig. 5 7-d Chilean OPC cured at 23 °C (*top*) and 10 °C (*bottom*), showing (in order of brightness), residual cement grains (*brightest*), portlandite (CH), C–S–H and AFm, and voids (*darkest*)

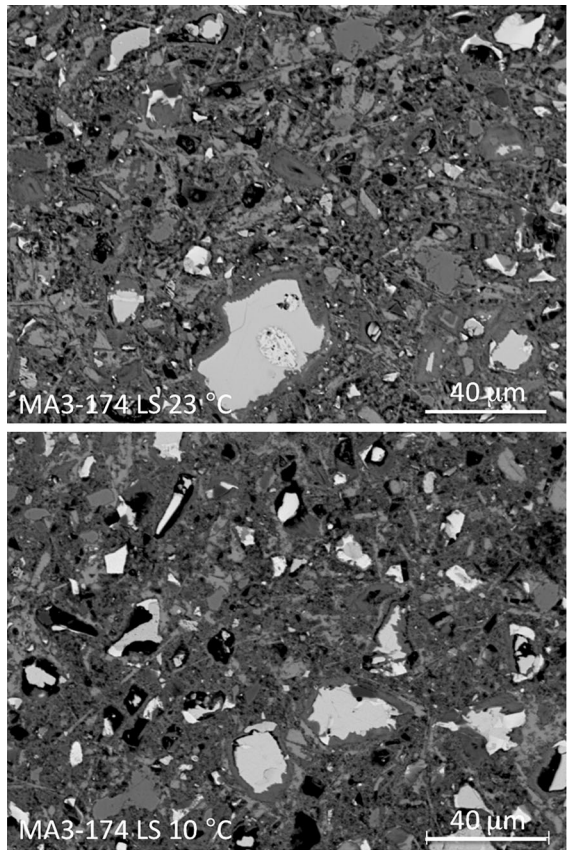

Fig. 6 PLC (10% LS) paste microstructure after 7 d curing at 23 °C (*upper*) and 10 °C (*lower*) appears to have a more finely-sized and uniformly distributed portlandite and for the 10 °C paste, a more dense-appearing C–S–H texture

forms. It is observed that as the temperature is lowered, the volume of calcite (remaining) is also reduced, due to its increased solubility at lower temperatures. In addition, an increase in the amount of AFt formed is observed at lower temperatures, likely due to the increased availability of carbonate anions in the pore solution. The amount of MC formed at lower temperatures is higher, while simultaneously the amount of $C_3(A,F)S_{0.84}H_{4.32}$ is reduced. Thus, more aluminates become available to form MC at lower temperatures. The same behavior is observed with portlandite and C-S–H compared to the Chilean OPC system. The total volume of solids difference between the 5 and 25 °C systems is 2.17%, attributed mainly to the additional AFt and MC formed at the lower temperature. The additional AFt predicted by the thermodynamic modeling is consistent with the XRD analysis presented earlier where there was some

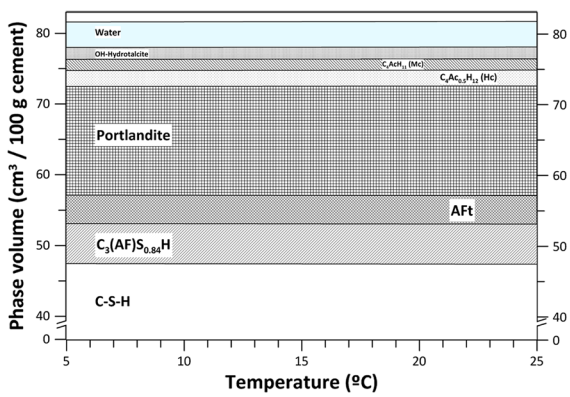

Fig. 7 Predicted phase assemblage at thermodynamic equilibrium as a function of curing temperature determined for Chilean OPC cement at a *w/c* of 0.4

indication of increased ettringite formation in the 10 °C PLC (10% LS) paste. Because the modeling predicts ultimate equilibrium phase distributions, it

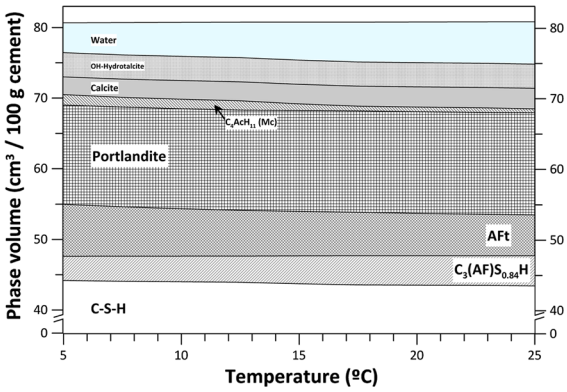

Fig. 8 Predicted phase assemblage at thermodynamic equilibrium as a function of curing temperature determined for PLC (10% LS) cement at a *w/c* of 0.4

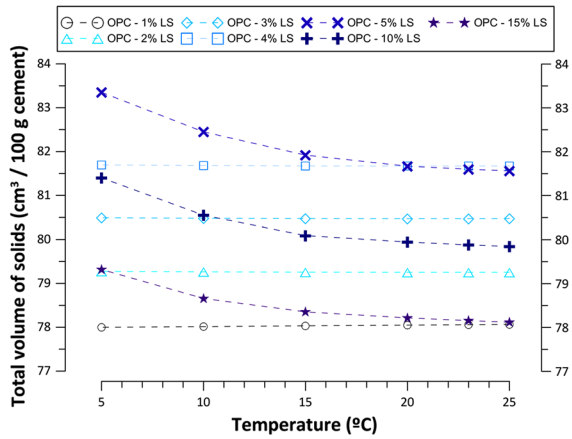

Fig. 9 Effect of temperature on the total volume of solids at thermodynamic equilibrium of Chilean OPC with different amounts of limestone replacements

does not predict the formation of the HC phase that was however observed in the PLC (10% LS) pastes by XRD analysis [15]. While MC may be favored thermodynamically over HC for PLC compositions [1], the latter may form first due to faster kinetics and later convert to the more (predicted) stable MC phase, explaining why more MC is observed at low temperature for an ultimate (equilibrium) state. This is not the case for the Chilean OPC, where HC is observed in the modeling results, as its CO_2/Al_2O_3 ratio (0.43) is significantly lower compared to that of the PLC. Still, overall in the PLC, a higher volume of solids is predicted at the lower curing temperatures by the thermodynamic modeling.

In order to further explore the influence of limestone on the increased formation of solid phases at lower temperatures, the Chilean OPC cement was used as a basis and different replacements of limestone were performed on a mass basis. Figure 9 shows the effect of temperature on the total volume of solids at thermodynamic equilibrium, with different amounts of limestone. At low OPC-by-limestone replacement levels (below 4%), no significant difference is observed between 5 and 25 °C curing. At these replacement levels, all of the available C $\overline{C}$ reacts with C_3A to form monocarbonate, thus, calcite behaves as a chemically reactive addition. In this case, the amount of AFt solid solution phase is smaller at low temperatures compared to higher ones, which is opposite to the behavior seen in Fig. 8. While the effect of temperature on the total volume of solids is negligible for this range of LS contents, the total amount of solids does increase with increasing replacement level, since the replacements were performed on a mass basis, and limestone is less dense than cement. In addition, the cement dilution is offset by the limestone being ultimately reactive when used at these low levels.

Conversely, at replacement levels of 5% and above, residual calcite is observed, and it starts behaving as an inert filler as well a reactive component. As additional calcite becomes available, the difference in solubility between low and high temperature starts playing a role, as additional AFt is formed at low temperatures. This is consistent with lower amounts of unreacted solid calcite being observed in the lower temperature models and in the experiments with the PLC (10% LS) pastes. The difference in the amount of AFt produced effectively offsets any negative effects of low temperature on the amounts of portlandite and C-S-H, and a higher total volume of solids is observed in comparison to higher temperatures. However, the total amount of solids tends to decrease in this range of replacement, regardless of these temperature effects, mainly due to the reduction in cement content (dilution).

At temperatures above 25 °C (modeling results not shown here), the thermodynamic model predicts a rapid destabilization of the MC and tricarboaluminate phases in all cements with LS, leading instead to the formation of conventional ettringite and an overall significant reduction (7–8%) in the total volume of solids compared to lower temperatures. While this could imply lower strengths at higher curing temperatures, this model prediction requires experimental

verification via further research. However, preliminary mortar testing at 40 °C has instead indicated similar strengths at 7 d for the PLC (10% LS) cement as those obtained at 10 and 23 °C (Table 3), while the Chilean OPC mortar with minimal limestone powder content exhibited its highest strength at 7 d for the 23 °C curing condition, with reductions of about 5 and 14% for the 10 and 40 °C curing, respectively. This implies a certain robustness with respect to curing temperature and strength for concretes containing limestone powder that could be a benefit for the variable curing temperatures commonly encountered in the field.

From the inspection of Fig. 9, it can be clearly seen that there is an optimal $C\overline{C}$ content for which the thermodynamic modeling predicts the highest volume of solids at equilibrium. This optimum is indeed the limit between a pure chemically active behavior of limestone (no solid limestone observed at equilibrium) and a mixture of chemical and physical effects (unreacted solid limestone observed). Since the solubility of $C\overline{C}$ and the uptake of CO_3^{2-} by ettringite are both higher at lower temperature, it is also expected that this optimum should be higher at a lower temperature, as more $C\overline{C}$ is required to saturate the pore solution. Figure 10 shows the effect of limestone content on the total volume of solids at 10 and 23 °C. For the Chilean OPC phase composition, an optimum of 4.15% by mass was determined for 23 °C curing and 4.35% for 10 °C (interestingly, both of these are near the 5% limit currently prescribed in ASTM C150). It can be seen that for limestone contents below the optimum value, there is no significant difference in the total volume of solids between low and high temperatures. However, for limestone contents above the optimum and typical of commercial PLCs with 10–15% LS, a lower curing temperature leads to the formation of a higher volume of solid phases and potentially a higher compressive strength, as observed for the PLC (10% LS) mortar in this study and as observed for other cements (OPC and blended) in a previous study [8]. The solid volume increase for limestone contents below the optimum value and the decreasing trend above it has also been observed recently for ternary and quaternary systems containing fly ash and blast-furnace slag apart from calcite [36].

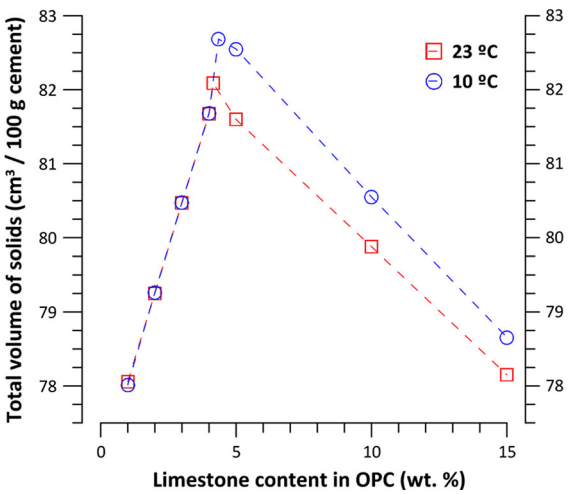

Fig. 10 Effect of limestone replacement level on the total volume of solids of Chilean OPC at 10 and 23 °C. The optimum is shown as the maximum for each temperature

6 Summary and prospectus

In contrast to OPC systems where phase assemblage is not typically a strong function of curing temperature, in PLC systems, curing temperature has a significant influence not only on hydration rates, but also on phase assemblage and resultant mechanical properties. One concrete example of this from the present study is the production of stronger mortar cubes after curing for only 7 d at 10 °C, as opposed to 23 °C. An examination of potential reactions and solubilities vs. temperature, along with thermodynamic modeling and TGA/XRD/SEM analysis, has indicated that the limestone powder not only contributes to the formation of HC and MC phases whose ratio varies with curing temperature, but also enhances ettringite formation at lower curing temperatures. The hypothesis of additional HC (less MC) and enhanced ettringite formation at lower curing temperatures is supported by the strength vs. heat release plots, the XRD analysis, and to a lesser extent, the thermodynamic modeling conducted in this study.

While this study has focused on mortars produced under controlled (and constant temperature) laboratory conditions, it has several implications for real world concreting. First, as witnessed previously with regards to setting times of HVFA mixtures [5], PLC systems may prove more robust with respect to cold weather concreting than their OPC counterparts. In the PLC systems, slower hydration kinetics can be

partially or totally offset by the greater volume of hydration products formed at the lower curing temperature; this is typically not the case with OPC systems. Second, the conventional application of the maturity method for predicting in situ strength development of field concretes may require modification when applied to PLC-based concretes. While an apparent activation energy approach may still provide an adequate description of the kinetics of reaction in a PLC-based concrete exposed to variable temperatures, the extension to predicting strength will require supplemental information on the total volume of solids being formed (porosity reduction) as a function of this maturity-predicted degree of hydration. XRD analysis and/or thermodynamic modeling should provide useful tools for performing this latter task.

Acknowledgements The authors would like to thank Todd Laker and Tim Cost of LafargeHolcim, Dr. Isaac Howard of Mississippi State University, and Larry Rowland of Lehigh Cement for their assistance in obtaining the cements investigated in the present study and Brett Philpotts of Lehigh Cement for providing XRF data. The assistance of Max Peltz of the Engineering Laboratory at NIST in providing the particle size distribution, BET surface area, and He pycnometry density data is gratefully acknowledged, as are useful discussions with Dr. Didier Lootens of Sika Technology, AG. The useful comments and suggestions of the journal reviewers are also appreciated.

Compliance with ethical standards

Conflict of interest The authors declare that they have no conflict of interest.

References

1. Matschei T, Lothenbach B, Glasser FP (2007) The role of calcium carbonate in cement hydration. Cem Concr Res 37:551–558
2. Chowaniec O (2012) Limestone addition in cement, Ph.D. Thesis, École Polytechnique Fédérale de Lausanne
3. Bentz DP, Tanesi J, Ardani A (2013) Ternary blends for controlling cost and carbon content. Concr Int 35(8):51–59
4. Oey T, Kumar A, Bullard JW, Neithalath N, Sant G (2013) The filler effect: the influence of filler content and surface area on cementitious reaction rates. J Am Ceram Soc 96(6):1978–1990
5. Bentz DP (2014) Activation energies of high-volume fly ash ternary blends: hydration and setting. Cem Concr Compos 53:214–223
6. Bentz DP, Ardani A, Barrett T, Jones SZ, Lootens D, Peltz MA, Sato T, Stutzman PE, Tanesi J, Weiss WJ (2015) Multi-scale investigation of the performance of limestone in concrete. Constr Build Mater 75:1–10
7. Bentz DP, Jones SZ, Lootens D (2016) Minimizing paste content in concrete using limestone powders—demonstration mixtures. NIST Technical Note 1906, U.S. Department of Commerce
8. Bentz DP, Zunino F, Lootens D (2016) Chemical vs. physical acceleration of cement hydration: $CaCl_2$ vs. limestone powder. Concr Int 38(11):53–60
9. Bentz DP, Ferraris CF, Jones SZ, Lootens D, Zunino F (2017) Limestone and silica powder replacements for cement: early-age performance. Cem Concr Compos 78:43–56
10. Plummer LN, Busenberg E (1982) The solubilities of calcite, aragonite, and vaterite in CO_2–H_2O Solutions between 0 and 90 C, and an evaluation of the aqueous model for the system $CaCO_3$–CO_2–H_2O. Geochim Cosmochim Acta 46:1011–1040
11. Bentz DP, Barrett T, De la Varga I, Weiss WJ (2012) Relating compressive strength to heat release in mortars. Adv Civil Eng Mater 1(1):14
12. Carino NJ, Lew HS (1983) Temperature effects on strength-maturity relations of mortar. ACI Mater J 80(3):177–182
13. Bentur A, Berger RL, Kung JH, Milestone NB, Young JF (1979) Structural properties of calcium silicate pastes: II, effect of curing temperature. J Am Ceram Soc 62(7–8):362–366
14. Lootens D, Bentz DP (2016) On the relation of setting and early-age strength development to porosity and hydration in cement-based materials. Cem Concr Compos 68:9–14
15. Hoshino S, Yamada K, Hirao H (2006) XRD/rietveld analysis of the hydration and strength development of slag and limestone blended cement. J of Adv Concr Technol 4(3):357–367
16. Dilnesa BZ, Lothenbach B, Le Saout G, Renaudin G, Mesbah A, Filinchuk Y, Wichser A, Weiland E (2011) Iron in carbonate containing AFm phases. Cem Concr Res 41:311–323
17. Berman HA, Newman ES (1961) Heat of formation of calcium aluminate monocarbonate at 25 °C. J Res Natl Bur Stand A Phys Chem 65A(3):197–207
18. Berman HA, Newman ES (1963) Heat of formation of calcium aluminate monosulfate at 25 °C. J Res Natl Bur Stand A Phys Chem 67(1):1–13
19. Houtepen CJM, Stein HN (1976) The enthalpies of formation and of dehydration of some afm phases with singly charged anions. Cem Concr Res 6:651–658
20. Bentz DP (1997) Three-dimensional computer simulation of portland cement hydration and microstructure development. J Am Ceram Soc 80(1):3–21
21. Puerta-Falla G, Balonis M, Le Saout G, Kumar A, Rivera M, Falzone G, Neithalath N, Sant G (2016) The influence of slightly and highly soluble carbonate salts on phase relations in hydrated calcium aluminate cements. J Mater Sci 51(12):6062–6074
22. Lothenbach B, Le Saout G, Gallucci E, Scrivener K (2008) Influence of limestone on the hydration of portland cements. Cem Concr Res 38:848–860
23. Moon J, Oh JE, Balonis M, Glasser FP, Clark SM, Monteiro PJM (2012) High pressure study of low compressibility

tetracalcium aluminum carbonate hydrates $3CaO{\cdot}Al_2O_3{\cdot}CaCO_3{\cdot}11H_2O$. Cem Concr Res 42:105–110
24. ASTM (2014) ASTM annual book of standards, vol. 04.01, Cement; Lime; Gypsum, ASTM International, West Conshohocken
25. Shannon J, Howard IL, Cost VT (2017) Potential of portland-limestone cement to improve performance of concrete made with high slag cement and fly ash replacement rates. J Test Eval 45(3):1–17. doi:10.1520/JTE20150306
26. Gurney L, Bentz DP, Sato T, Weiss WJ (2012) Reducing set retardation in high volume fly ash mixtures with the use of limestone: improving constructability for sustainability. Transp Res Rec J Transp Res Board, No. 2290, Concr Mater 139–146
27. Bentz DP, Ferraris CF (2010) Rheology and setting of high volume fly ash mixtures. Cem Concr Compos 32(4):265–270
28. Stutzman PE, Clifton JR (1999) Specimen preparation for scanning electron microscopy. In: Proceedings of the 21st international conference on cement microscopy, Las Vegas, NV, 10–22
29. Guide to compounds of interest in cement and concrete research (1972). Special Report 127, Highway Research Board, National Research Council, 53 pp
30. Kulik DA, Wagner T, Dmytrieva SV, Kosakowski G, Hingerl FF, Chudnenko KV, Berner U (2013) GEM-Selektor geochemical modeling package: revised algorithm and GEMS3K numerical kernel for coupled simulation codes. Comput Geosci 17:1–24
31. Wagner T, Kulik DA, Hingerl FF, Dmytrieva SV (2012) GEM-Selektor geochemical modeling package: tSolMod library and data interface for multicomponent phase models. Can Miner 50:701–723
32. Lothenbach B, Matschei T, Möschner G, Glasser FP (2008) Thermodynamic modelling of the effect of temperature on the hydration and porosity of Portland cement. Cem Concr Res 38:1–18
33. Matschei T, Glasser FP (2010) Temperature dependence, 0 to 40 C, of the mineralogy of Portland cement paste in the presence of calcium carbonate. Cem Concr Res 40:763–777
34. Bentz DP (2000) CEMHYD3D: a three-dimensional cement hydration and microstructure development modelling package. Version 2.0. NISTIR 6485, U.S. Department of Commerce
35. Dilnesa BZ, Lothenbach B, Renaudin G, Wichser A, Kulik D (2014) Synthesis and characterization of hydrogarnet $Ca_3(Al_xFe_{1-x})_2(SiO_4)_y(OH)_{4(3-y)}$. Cem Concr Res 59:96–111
36. Schöler A, Lothenbach B, Winnefeld F, Zajac M (2015) Hydration of quaternary Portland cement containing blast-furnace slag, siliceous fly ash and limestone powder. Cem Concr Compos 55:374–382